Electronic Supplementary Material (ESI) for Chemical Science.

Supporting information

The promotional role of Mn in CO_2 hydrogenation over Rh-based catalysts from a surface organometallic chemistry approach

Wei Zhou, Scott R. Docherty, Christian Ehinger, Xiaoyu Zhou, and Christophe Copéret*

Department of Chemistry and Applied Biosciences, ETH Zürich, CH-8093 Zurich, Switzerland

*Corresponding author: ccoperet@inorg.chem.ethz.ch

Experimental and details

General procedure

Unless otherwise stated, all the operations of catalysts were carried out in a M. Braun glovebox (Argon) or using high vacuum standard Schlenk techniques (Argon). Pentane was dried using a MB SPS 800 solvent purification system, where columns were packed with activated copper and alumina for pentane purification. Benzene was either distillated from purple Na^0/benzophenone or obtained from MB SPS system. Deuterated benzene (C_6D_6) was distilled from Na^0/benzophenone. All the solvents were stored over 4 Å molecular sieves in the glovebox. Diisopropylcarbodiimide (Sigma Aldrich), MeLi in Et_2O (Sigma Aldrich) (1.73 M), and Chloro(1,5-cyclooctadiene) rhodium(I) dimer (abcr GmbH) were used as received. To prepare the SiO_2 dehydroxylated at 700 °C (denoted as $SiO_{2\text{-}700}$), Commercial silica (Aerosil® 200 from Evonik) was first treated by wetting with water to form a slurry and dried at 100 °C for several days in an oven to obtain the large agglomerates. These agglomerates were compacted and sieved to select the particles with sizes of 250-420 μm (40-60 Mesh). 2 g of as-prepared silica was calcined at 500 °C in static air for 8 h (ramp: 5 °C/min) and then evacuated under high vacuum (10^{-5} mbar) for another 8 h at the same temperature. Subsequently, the temperature was further heated up to 700 °C for 24 h (ramp: 1 °C/min) to obtain $SiO_{2\text{-}700}$. The density of silanols of $SiO_{2\text{-}700}$ was titrated with $Mg(CH_2Ph)_2(THF)_2$ and quantified by solution ^1H NMR (200 MHz, 25 °C, d1 = 58 sec) in presence of ferrocene as internal standard. The density of –OH was determined to 0.28 mmol/g, corresponding to 0.86 –OH/nm^2. $[Mn_2(OSi(O\textit{t}Bu)_3)_4]$ was synthesized according to the literature procedure [1] and stored in glovebox (Argon).

Rh molecular precursor synthesis

To synthesize the (N,N'-diisopropylacetamidinate)(1,5-cyclooctadiene)rhodium (abbreviated as Rh(COD)(DIA))precursor, Li(DIA)(THF) needs to be prepared first. Synthesis of Lithium N,N'-

diisopropylacetamidinate (Li(DIA)) [2]: Diisopropylcarbodiimide (3.95 g, 31.3 mmol, 1.05 equiv) was added to a flame dried Schlenk flask under Ar, which was then purged with Ar for about 1 minute. Et_2O (50 mL) was added via canula, and the solution was cooled to -40 °C using an acetonitrile/dry ice bath. A 1.73 M solution of MeLi in Et_2O (17.2 mL, 29.8 mmol, 1.00 equiv.) was added dropwise while stirring. The mixture was then allowed to reach room temperature and stirred for 2 hours. The volatiles were removed in vacuo to yield Li(DIA) as a white powder. The crude product was recrystallized by redissolving it in THF (ca. 10 mL), layering this solution with pentane (ca. 5 mL) and cooling to -40 °C. Successive crystallization from the mother liquor yielded the THF adduct of Li(DIA) as large, colorless crystalline blocks. Combined yield of three crops: 4.8 g (73%). Crystals suitable for X-Ray diffraction were obtained using the same approach. **^{1}H NMR (500 MHz, C_6D_6):** δ 3.58 (m, *J* = 6.2 Hz, 2H), 3.51 (t, *J* = 6.4 Hz, 4H), 1.86 (s, 3H), 1.37 (m, *J* = 3.2 Hz, 4H), 1.27 (d, *J* = 6.2 Hz, 12H) (Figure S1). **^{13}C NMR (126 MHz, C_6D_6):** δ 170.0, 67.7, 47.7, 26.6, 25.6, 11.9 (Figure S2).

Synthesis of (N,N'-diisopropylacetamidinate)(1,5-cyclooctadiene)rhodium (Rh(COD)(DIA)):
In an Ar filled glovebox, Chloro(1,5-cyclooctadiene) rhodium(I) dimer (101 mg, 0.205 mmol, 1.0 equiv. Rh) and Li-DIA(THF) (90.1 mg, 0.409 mmol, 1.0 equiv) were weighed in a Schlenk flask. Pentane (15 mL) was added, and the mixture was stirred for 18 hours at room temperature. The precipitated LiCl was removed from the yellow solution by filtration over celite. The filtrate was concentrated to dryness yielding a crude yellow powder which is almost pure at this stage (by ^{1}H NMR spectroscopy). The crude product could be purified by crystallization from pentane. It was redissolved in pentane (ca. 3 mL), and cooled to -40 °C. After collecting the first crop, the mother liquor was concentrated further and cooled to -40 °C again. Repeating this procedure two more times afforded the title compound as yellow crystalline solid. Combined yield of three crops: 130 mg (90%). **^{1}H NMR (500 MHz, C_6D_6):** δ 4.47 (s (br), 4H), 3.19 (heptd, $^3J_{H\text{-}H}$ = 6.4 Hz, $^3J_{Rh\text{-}H}$ = 2.4 Hz, 2H), 2.37 – 2.24 (m, 4H), 1.65 – 1.50 (m, 4H), 1.34 (s, 3H), 0.94 (d, *J* = 6.4 Hz, 12H) (Figure S4). **^{13}C NMR (126 MHz, C_6D_6):** δ 178.7 (d,$^2J_{Rh\text{-}C}$ = 4.2 Hz), 75.3 (d,$^1J_{Rh\text{-}C}$ = 12.3 Hz), 48.2 (d,$^2J_{Rh\text{-}C}$ = 2.1 Hz), 31.4, 25.1, 10.6 (Figure S5). **IR (ATR, cm^{-1}):** 3015, 2964, 2922, 2874, 2828, 1473, 1371, 1337, 1309, 1233, 1212, 1173, 1136, 1119, 983 (Figure S6). **Elemental analysis:** calculated based on $C_{16}H_{29}N_2Rh$: C 54.5%, H 8.3%, N 8.0%; found: C 54.5%, H 8.2%, N 8.0%.

Synthesis of $Rh@SiO_2$ and $RhMn@SiO_2$:

1.0 g of $SiO_{2\text{-}700}$ or $Mn^{II}@SiO_2$ was added to a 50 mL Schlenk flask. Benzene (about 5 mL) was added to give a white suspension. A solution of Rh(COD)(DIA) (88 mg, 0.25 mmol) in benzene (10 mL) was dropwise added to the suspension, then stirred for 4 h. The suspension was rinsed with benzene (5 mL) three times and with pentane once (5 mL). The benzene washings were combined, and further analyzed by using ^1H NMR spectroscopy (200 MHz, 25 ^oC, d1 = 58 sec) using ferrocene as an internal standard. No starting material was observed in the washings. The material was subsequently dried under high vacuum (10^{-5} mbar) for 1 h to yield Rh(COD)(DIA)$@SiO_2$ or Rh(COD)(DIA) Mn^{II} $@SiO_2$, followed by H_2 treatment at 400 ^oC (Ramp: 1 ^oC/min) for 5 h to remove all organics. The obtained $Rh@SiO_2$ and $RhMn@SiO_2$ samples were subsequently stored in glovebox (Argon).

Catalyst characterization

Elemental analysis of $Rh@SiO_2$ and $RhMn@SiO_2$ were measured by the Mikroanalytisches Labor Pascher, Remagen, Germany; while the C, H, N of Rh(COD)(DIA) were analyzed by the Mikroanalytisches Labor at ETH. Catalyst morphology was assessed by transmission electron microscopy (TEM) on a JEOL HEM-1400 Plus microscope within the facilities of ScopeM at ETH Zurich. The particle size distribution were determined by counting above 100 individual particles, and the average size and standard deviation are determined by a normal distribution function.

Solution ^1H-NMR and ^{13}C-NMR were collected on BrukerR DRX 500 spectrometer (11.75 T, Larmor Frequency: 500 MHz(^1H), 126 MHz (^{13}C)) in deuterated benzene (C_6D_6). The chemical shifts are referenced based on the solvent peaks.[3] Chemical shifts are reported in parts per million (ppm) and coupling constants ($^NJ_{X\text{-}X}$) are given in Hertz (Hz). Where appropriate, signal multiplicity has

been condensed to a single letter format, i.e.: s=singlet, d=doublet, t=triplet, q=quartet, m=multiplet. Solid-state NMR spectra of grafted samples were recorded on a Bruker 400 MHz NMR spectrometer using a double resonance 3.2 mm probe. Samples were packed in 3.2 mm zirconia rotors inside an Ar-filled glovebox, and spectra were recorded at 25 ^{o}C with a spinning speed of 16 kHz, using N_2 as gas for both bearing and drive. The downfield ^{13}C resonance of adamantane (38.5 ppm) was used as an external secondary reference to calibrate chemical shifts.

H_2/CO chemisorption experiment were performed on a Belsorb-Max instrument from BEL Japan. In an air-tight measuring cell, approximately 100 mg of reduced catalyst was loaded inside the glovebox (Argon) and then mounted on the apparatus. The sample was pre-treated at 300 ^{o}C for 1 h at 10^{-5} mbar. Adsorption isotherm measurements were performed at 25 ^{o}C. In all cases, the pressures variation was below 0.6% for 1200 seconds. For the H_2 chemisorption, the uptake was calculated from the adsorption at saturation deriving from a dissociative Langmuir adsorption function model. For the CO chemisorption, the uptake was calculated from the adsorption at saturation deriving from a double Langmuir adsorption function model.

Fourier-Transform Infrared (FTIR) spectroscopy experiments were performed on self-supporting wafers using a Bruker Alpha FT-IR spectrometer in transmission mode (24 scans, 4 cm^{-1} resolution) under air-free condition. CO-FTIR measurements were carried out on Nicolet 6700 FTIR instrument. Typically, a self-supporting pellet of Rh-based catalysts was exposed to CO atmosphere with different pressures and evacuated (10^{-5} mbar) for 15 min at room temperature. The spectra were collected from 4000 to 600 cm^{-1} at a resolution of 2 cm^{-1} in transmission mode. Spectra are normalized to Si-O-Si overtone peak maximum at 1868 cm^{-1} for all the materials. *In situ* high-pressure diffuse reflectance infrared Fourier-transform spectroscopy (DRIFTS) measurements were carried out on an FTIR spectrometer (Thermo Fisher iS50) equipped with liquid nitrogen N_2 cooled mercury–

cadmium–telluride (MCT) detector. The spectra were recorded from 4000 to 600 cm^{-1}. The catalyst powders were placed in a high-pressure (0–10 MPa) DRIFTS cell (Harrick) equipped with ZnSe windows. Prior to each measurement, the sample was pretreated in pure H_2 (20 mL min^{-1}) at 400 ^oC for 1 h. Then, the sample was cooled to 230 ^oC, followed by pressurizing to 20 bar with H_2/Ar (3:2). After recording the background spectrum, a CO_2/H_2/Ar (1:3:1) gas at 20 bar was switched into the *in situ* DRIFTS cell at 230 ^oC, and the evolution of IR spectra was recorded.

In-situ X-ray adsorption spectroscopy (XAS) experiments were measured at BM31 of the Swiss-Norwegian Beamlines (SNBL) located at the European Synchrotron Radiation Facility (ESRF) in Grenoble, France. Rh K-edge and Mn K-edge were collected in transmission mode using a double crystal Si (111) monochromator. In each case, the ionization chambers were filled with a gas mixture optimized for the edge energy and path length required. For each edge, a secondary reference for energy calibration was used (Rh foil and Mn foil). Typical beam dimensions used were 0.4 mm (H) x 4 mm (W), and beam size was controlled using slits. The sample was packed into quartz capillary (1.5 mm for Rh K-edge, 1.0 mm for Mn K-edge), in each case, a catalyst bed ca. 1 cm in length was used, and the powdered sample was secured using quartz wool plugs at each end. The packed capillary was loaded into a cell and isolated from exterior environment using two three-way Swagelok valves with an integrated bypass. [4] For acquisition of EXAFS, spectra were collected at beam energies range from 23.1-24.1 keV for the Rh K, and from 6.4-7.1 keV for the Mn K. 4 scans for Rh K-edge and 16 scans for Mn K-edge were averaged to obtain a sufficient quality for the structural analysis. The acquisition time for XANES and EXAFS at Rh K-edge were ca. 0.5 and 2 minutes respectively, while at Mn K-edge were ca. 1 and 3 minutes respectively. Flow rates (Ar, H_2, CO_2) were controlled using mass-flow controllers (Bronkhorst), and pressure was set at 20 bar using a back pressure regulator (Bronkhorst, EL-PRESS).Throughout the experiments, a flow of 10 mL min^{-1} was

maintained, and the outlet gas was monitored using a mass spectrometer to ensure that the similar chemistry proceeds over catalysts. After pressurization, the baseline shift, associated with the introduction/removal of a fraction of Ar was used to assess when composition of feed gas evolved at the catalyst bed, using a strategy similar to that described by Lomachenko et al. [5] The temperature for H_2 reduction (400 ^oC) and CO_2 hydrogenation (230 ^oC) were maintained using a nitrogen blower. Prior to measurements, a K-type thermocouple mounted inside a sample cell was used for the temperature calibration.

In a typical experiment, EXAFS spectra were first collected after the sample was mounted and exposed to air (Figure S20). Subsequently, H_2 pretreatment was carried out under 10 mL min^{-1} of H_2 for 1 h at 400 ^oC (300 ^oC h^{-1} ramp), while continuously collecting XANES spectra. After cooling to room temperature (or < 50 ^oC) under a flow of H_2, EXAFS spectra were collected for the reduced sample. Then, heating to reaction temperature (230 ^oC) under 10 mL of H_2/Ar (3:2) mixture (300 ^oC h^{-1} ramp), followed by pressurizing to 20 bar and retaining this condition for 20 min. Subsequently, the gas composition was switched to CO_2/H_2/Ar (1:3:1) mixture for CO_2 hydrogenation and the condition was retained for 2 h. Notably, the XANES spectra were continuously collected during the entire reaction protocol. After CO_2 hydrogenation, the gas was switched to Ar and the sample was cooled to room temperature for the post-CO_2-hydrogenation EXAFS spectra. Regarding the bimetallic RhMn sample, Rh and Mn K-edge XAS spectra were separately collected under the identical *in situ* conditions due to the significant difference in beam energies. Demeter software (0.9.24) from the Ifeffit software package (Version 1.2.11) was used for the XAS data analysis. [6]

Catalyst evaluation

CO_2 hydrogenation reactions were carried out on a fixed-bed flow reactor (PID Eng&Tech). Typically,

appropriate amount of catalyst (30 mg and 125 mg for $Rh@SiO_2$ and $RhMn@SO_2$, respectively) was mixed with 4.0 g of SiC and packed in the reactor in air. Prior to the CO_2 hydrogenation, the catalyst was reduced at 1 bar under 50 mL min^{-1} of H_2 for 1 h at 400 ^oC (10 ^oC/min ramp). After reduction, the furnace was cooled down to the reaction temperature (230 ^oC), and the reactor pressurized to the reaction pressure (40 bar) under the reacting gas flow (80 mL min^{-1} of 1:3:1 CO_2:H_2:Ar). The effect of conversion on product formation rates was probed by systematically varying the total gas flow rate from 6 mL min^{-1} to 100 mL min^{-1}. Finally, activity data was collected again at the initial flow rate to check for potential catalyst deactivation. The effluent gases were analyzed via online gas chromatography (Agilent 7890B equipped with Restek Rt-U-BOND (30 m x 0.53 mm x 20 μm) and Rt-Msieve 5A (30 m x 0.53 mm x 50 μm) columns) and quantified by a flame ionization detector (FID) for CH_3OH, C_2H_5OH and C_{2+} hydrocarbons) and thermal conductivity detector (TCD) for Ar, CO_2, CO and CH_4. GC data was collected in increments of half an hour.

The CO_2 conversion and product selectivity were calculated using the following set of equations:

$$S_x = \frac{F_{X,out}}{\sum_{i=1}^{n} F_{i,out}}$$

$$X_{CO2} = \frac{\sum_{i=1}^{n} F_{i,out}}{F_{CO2,in}}$$

Product selectivity (S_x) is defined as the outflow of the component in equation, $\sum_{i=1}^{n} F_{i,out}$, divided by the sum of of outlet flows for all carbon containing products, $\sum_{i=1}^{n} F_{i,out}$. The CO_2 conversion (X_{CO2}) is defined as the sum of outlet flows for all the carbon containing products, $\sum_{i=1}^{n} F_{i,out}$, divided by the inlet flow of CO_2, $F_{CO2,in}$. Note that all concentrations are normalized per carbon to enable accurate comparison.

Supporting figures and tables

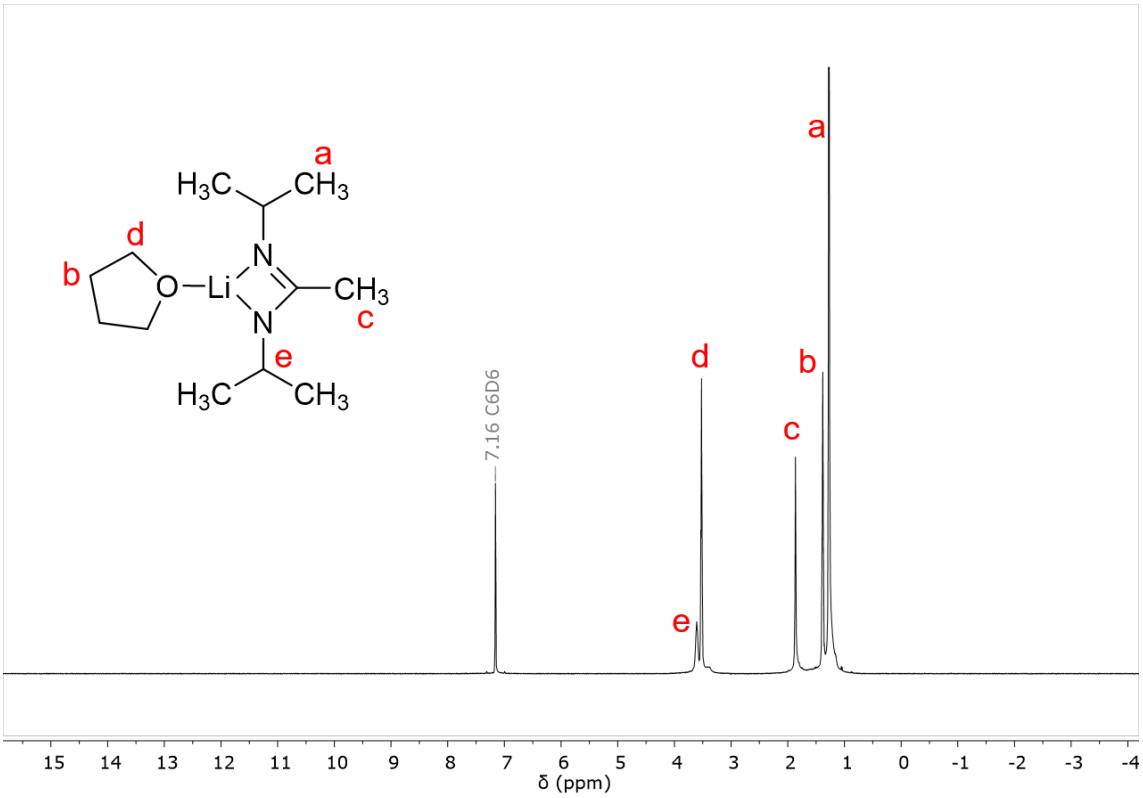

Figure S1. The proton solution NMR results for the Li-DIA(THF). (500 MHz, C_6D_6, 25 ^oC)

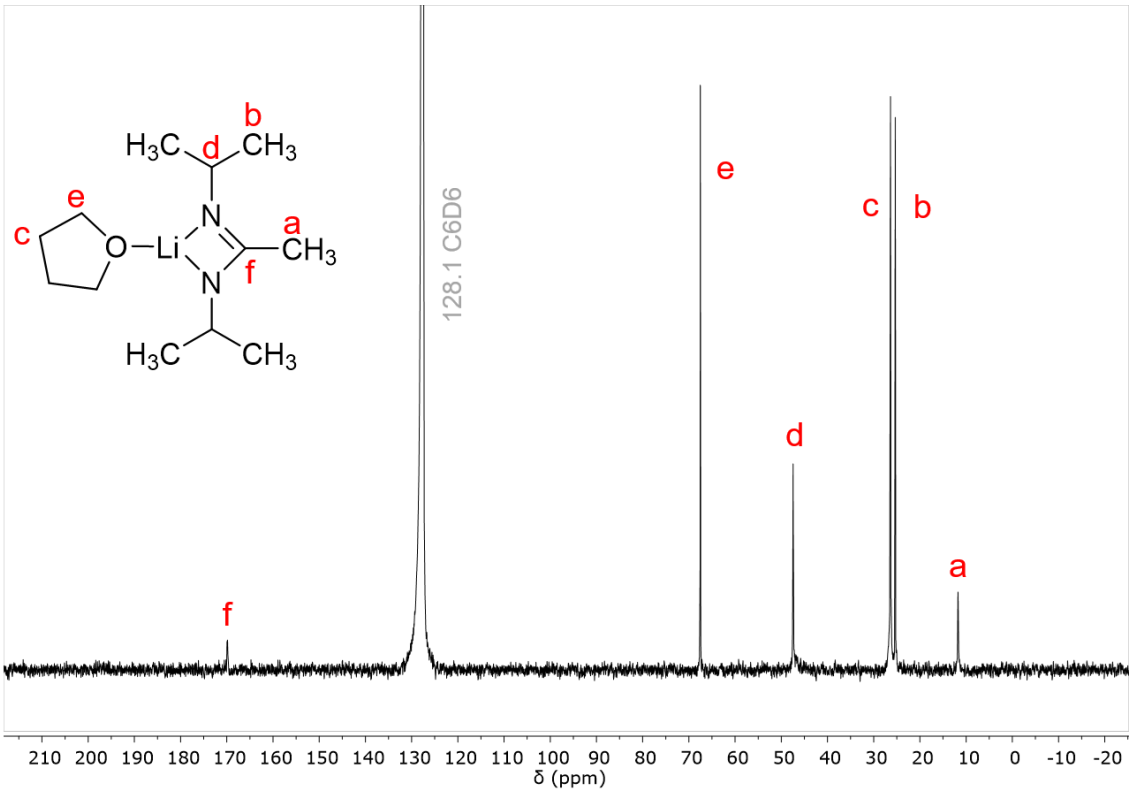

Figure S2. The ^{13}C solution NMR results for the Li-DIA(THF). (126 MHz, C_6D_6, 25 ^{o}C)

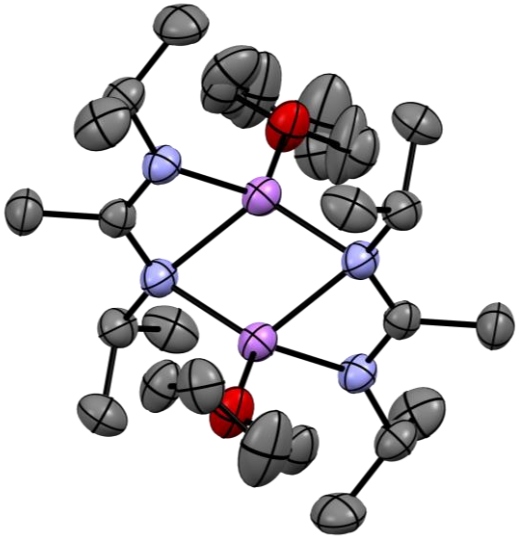

Figure S3. Crystal structure for Li-DIA(THF). Ellipsoids shown at 50% probability, hydrogens omitted for clarity

Single crystal of $C_{12}H_{25}LiN_2O$ (Li-DIA(THF)) were crystallized from THF and Pentane at -40 ºC overnight. A suitable crystal was selected and tip-mounted on a MiTeGen Pin covered with Paratone Oil on a XtaLAB Synergy, Dualflex, HyPix diffractometer. The crystal was kept at 200.15 K during data collection. Using Olex2 [7], the structure was solved with the SHELXT [8] structure solution program using Intrinsic Phasing and refined with the SHELXL [9] refinement package using CGLS minimisation.

Crystal Data for $C_{12}H_{25}LiN_2O$ (M =220.28 g/mol): triclinic, space group P-1 (no. 2), a = 9.5338(2) Å, b = 10.5863(3) Å, c = 14.6615(5) Å, α = 91.507(2)°, β = 97.369(2)°, γ = 101.367(2)°, V = 1436.72(7) Å^3, Z = 4, T = 200.15 K, μ(Cu Kα) = 0.487 mm^{-1}, *Dcalc* = 1.018 g/cm^3, 50271 reflections measured (6.086° ≤ 2Θ ≤ 161.202°), 6190 unique (R_{int} = 0.0271, R_{sigma} = 0.0135) which were used in all calculations. The final R_1 was 0.0472 (I > 2σ(I)) and wR_2 was 0.1396 (all data).

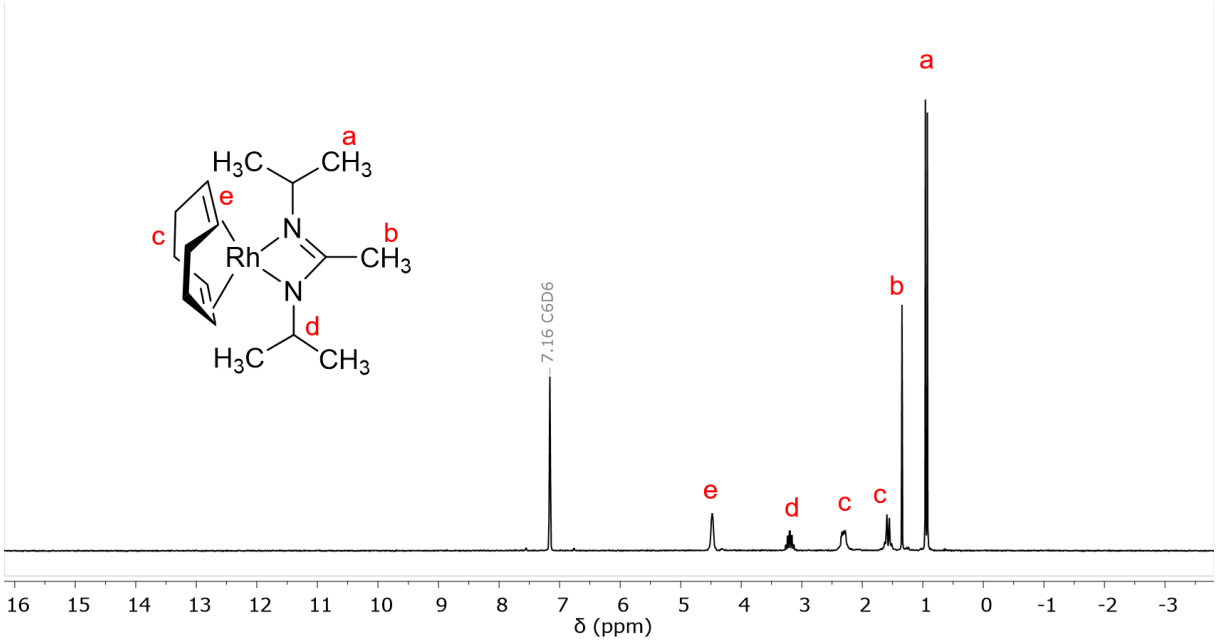

Figure S4. The proton solution NMR results for the Rh(COD)(DIA) precursor. (500 MHz, C_6D_6, 25 ^oC)

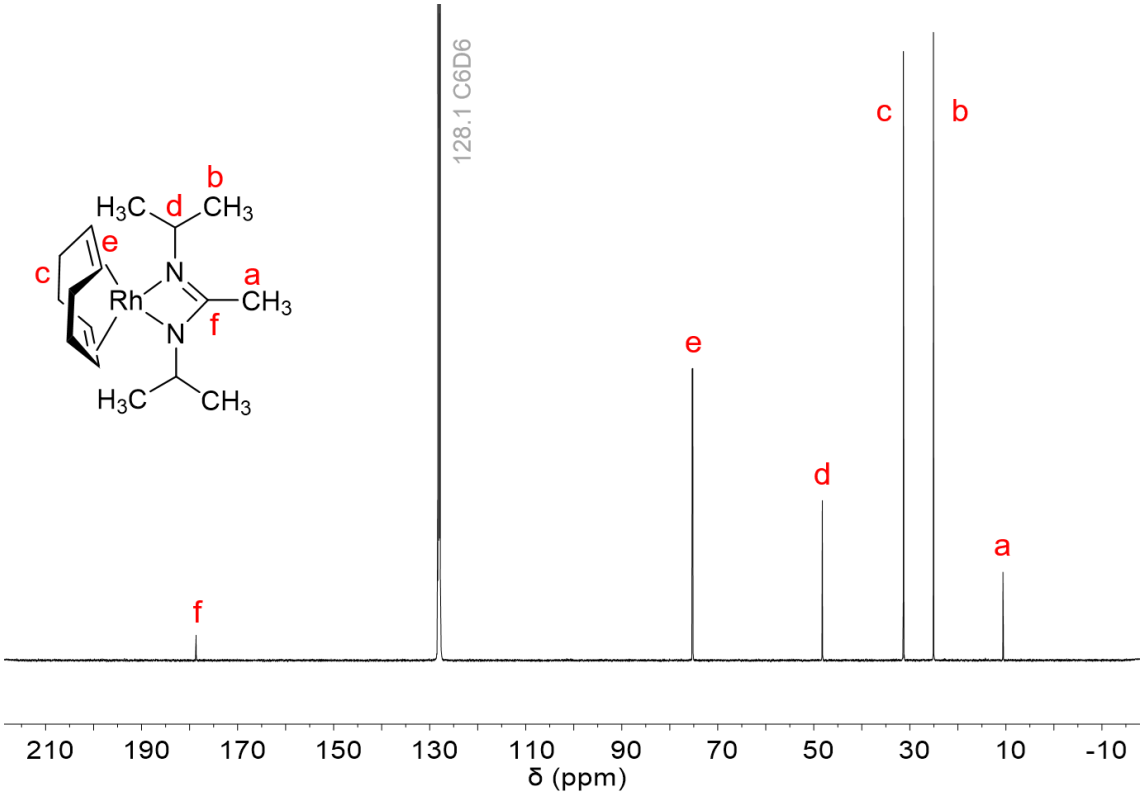

Figure S5. The ^{13}C solution NMR results for the Rh(COD)(DIA) precursor. (126 MHz, C_6D_6, 25 ^{o}C)

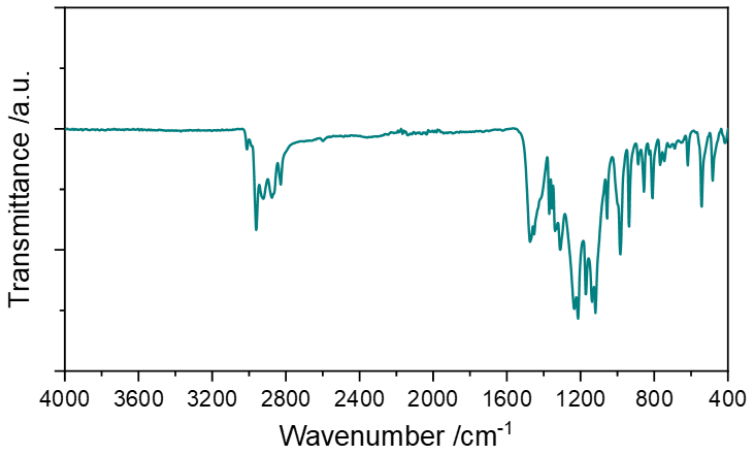

Figure S6. ATR-IR of Rh(COD)(DIA) precursor. Transmittance range: 4000-400 cm^{-1}.

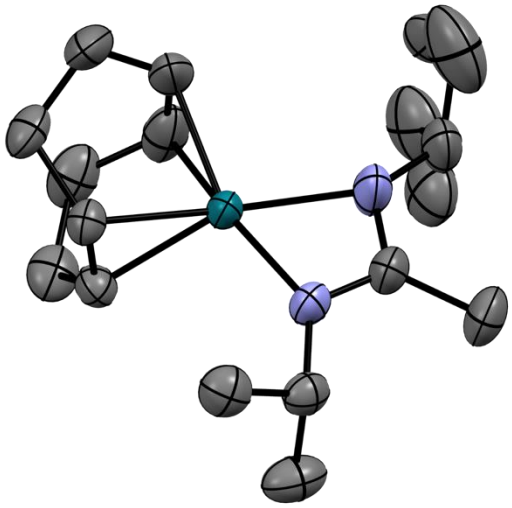

Figure S7. Crystal structure for Rh(COD)(DIA). Ellipsoids shown at 50% probability, hydrogens omitted for clarity. Note that upper right of isopropyl group split due to disorder.

Single crystals of $C_{16}H_{29}N_2Rh$ were crystallized from Pentane at -40 ºC overnight. A suitable crystal was selected and tip-mounted on a MiTeGen Pin covered with Paratone Oil on a XtaLAB Synergy, Dualflex, HyPix diffractometer. The crystal was kept at 230.00(10) K during data collection. Using Olex2 [7], the structure was solved with the olex2.solve [10] structure solution program using Charge Flipping and refined with the SHELXL [9] refinement package using CGLS minimization

Crystal Data for $C_{16}H_{29}N_2Rh$ (M =352.32 g/mol): orthorhombic, space group Pbca (no. 61), a = 10.7527(4) Å, b = 10.0218(3) Å, c = 30.3983(11) Å, V = 3275.8(2) Å^3, Z = 8, T = 230.00(10) K, μ(Cu Kα) = 8.329 mm^{-1}, *Dcalc* = 1.429 g/cm^3, 24606 reflections measured (5.814° ≤ 2Θ ≤ 160.27°), 3541 unique (R_{int} = 0.0468, R_{sigma} = 0.0231) which were used in all calculations. The final R_1 was 0.0364 (I > 2σ(I)) and wR_2 was 0.1038 (all data).

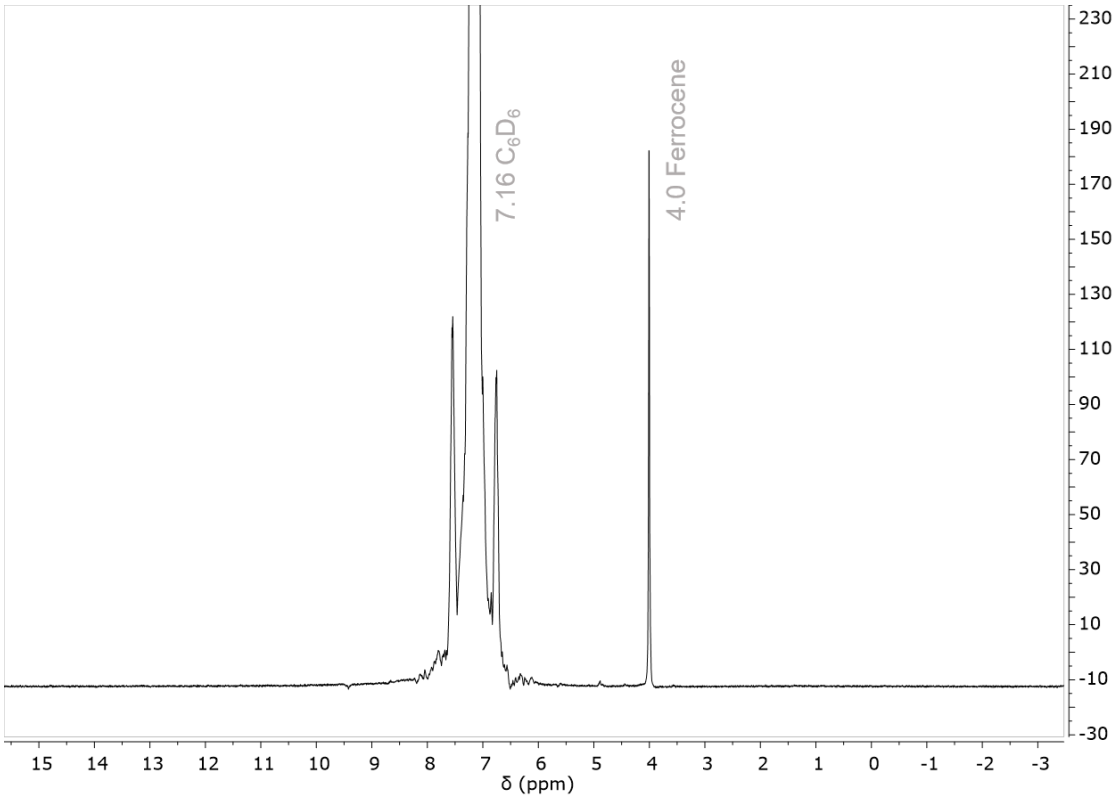

Figure S8. The proton solution NMR results for washings after the Rh(COD)(DIA) grafted on $SiO_{2\text{-}700}$.

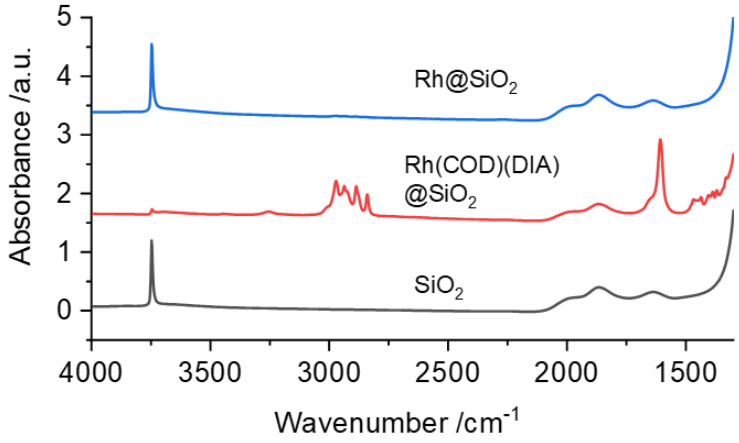

Figure S9. IR spectra throughout the synthesis of $Rh@SiO_2$.

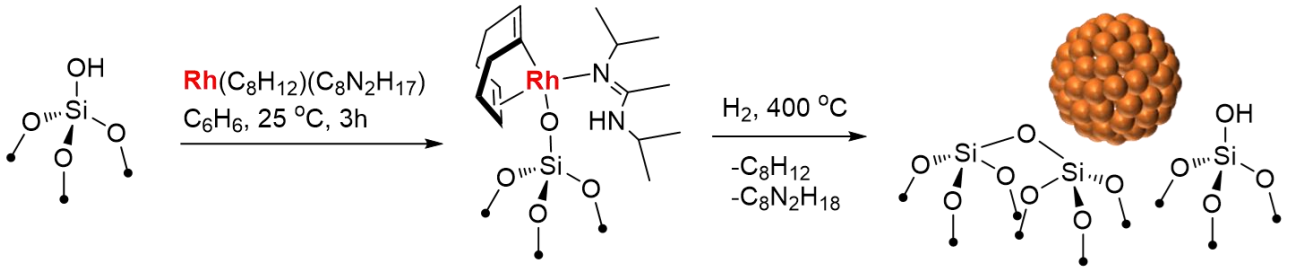

Figure S10. Schematic procedure for grafting of Rh(COD)(DIA) on $SiO_{2\text{-}700}$ followed by reduction under H_2 at 400 °C.

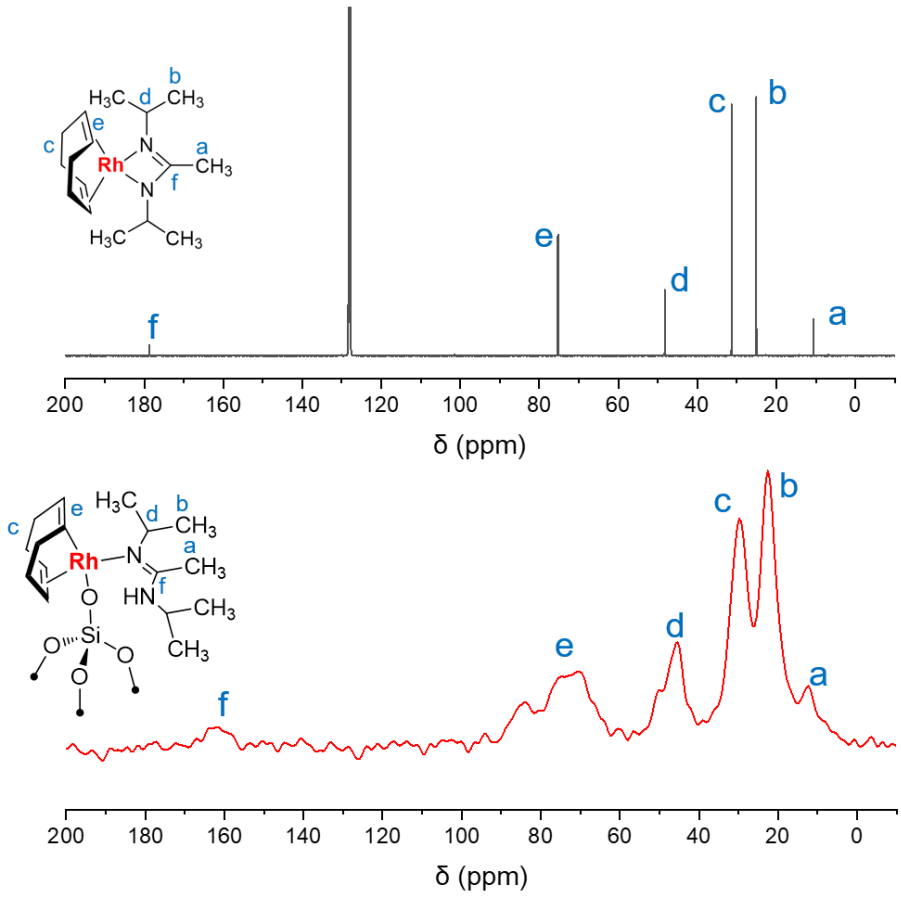

Figure S11. ^{13}C solution NMR spectra for Rh(COD)(DIA) in C_6D_6 and ^{13}C CP-MAS for Rh(COD)(DIA)@SiO_2.

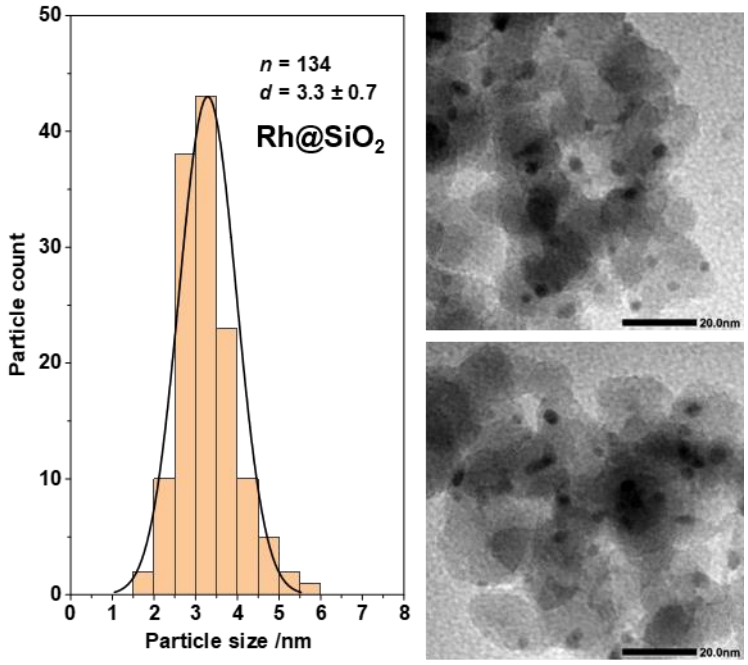

Figure S12. Particle size distribution and TEM images of $Rh@SiO_2$.

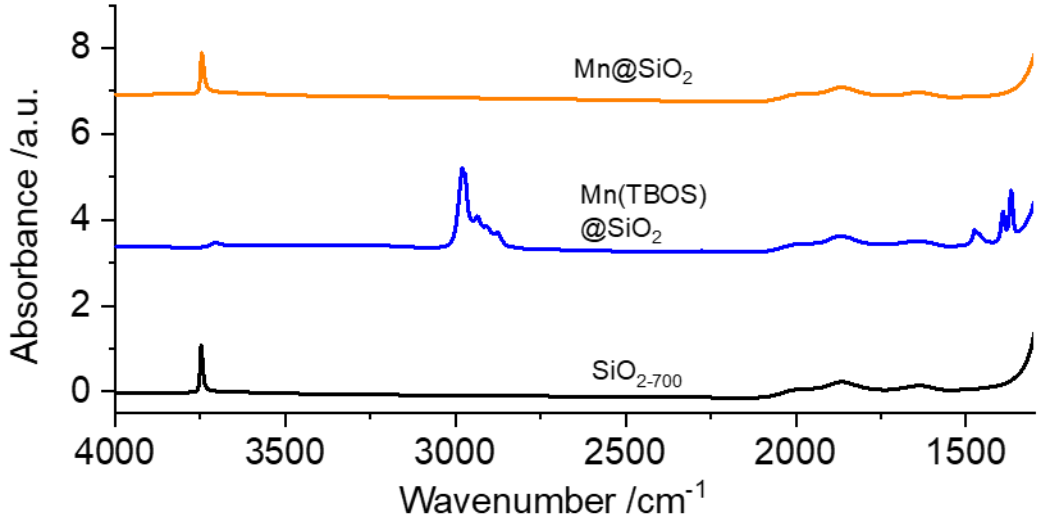

Figure S13. IR spectra throughout the synthesis of $Mn@SiO_2$.

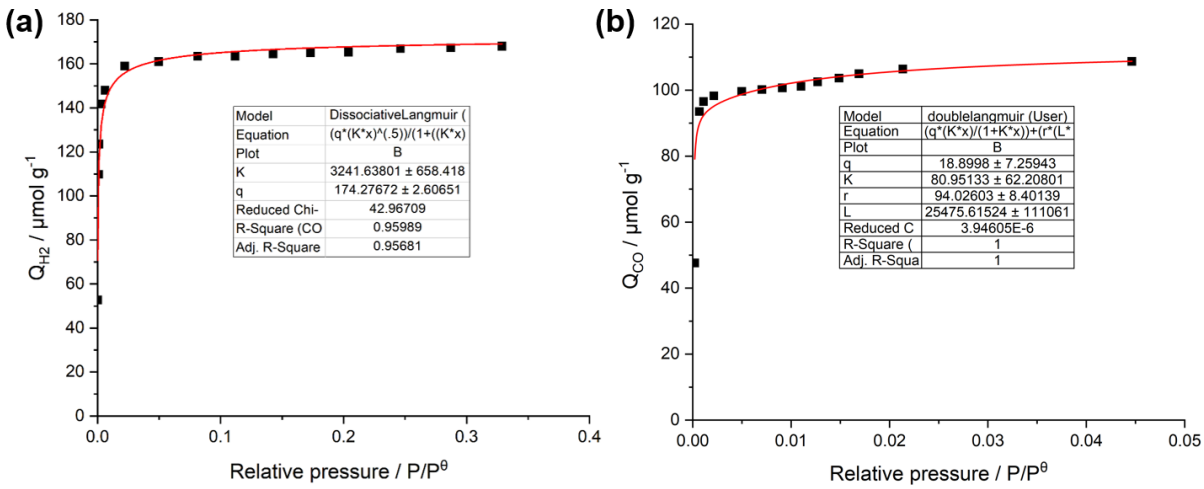

Figure S14. H_2 chemisorption isotherm (a) and CO chemisorption isotherm (b) for $Rh@SiO_2$.

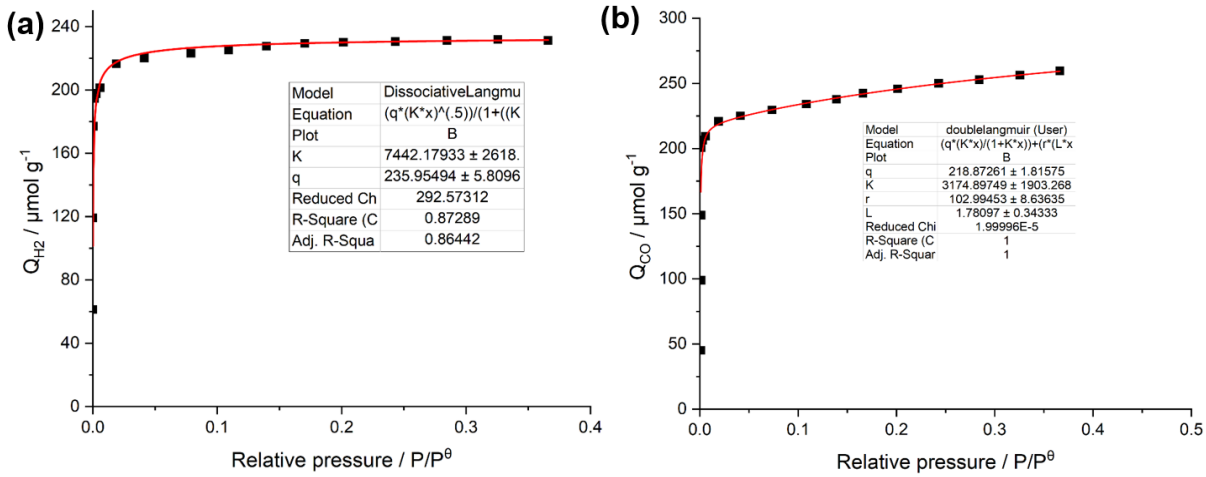

Figure S15. H_2 chemisorption isotherm (a) and CO chemisorption isotherm (b) for $RhMn@SiO_2$.

Table S1. Physicochemical properties of as-synthesized catalysts.

Catalyst	EA (wt%)	Particle size (nm)[a]	H_2 chemisorption (mol_{CO} mol_{Rh}^{-1})	CO chemisorption mol_{H2} mol_{Rh}^{-1}	H/Rh	CO/Rh
$Rh@SiO_2$	Rh: 2.26	3.3 ± 0.7	0.79	0.51	1.58	0.51
$RhMn@SiO_2$	Rh: 2.34 Mn: 1.45	1.9 ± 0.5	1.04	1.41	2.08	1.41

[a] particle size determined by TEM.

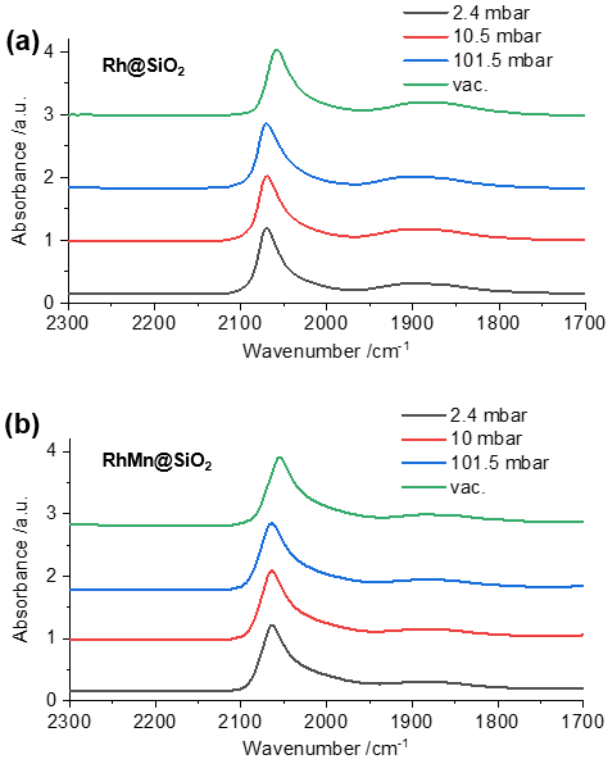

Figure S16. FTIR spectra of CO adsorbed on $Rh@SiO_2$ (a) and $RhMn@SiO_2$ (b) under different CO pressures and after evacuating at room temperature.

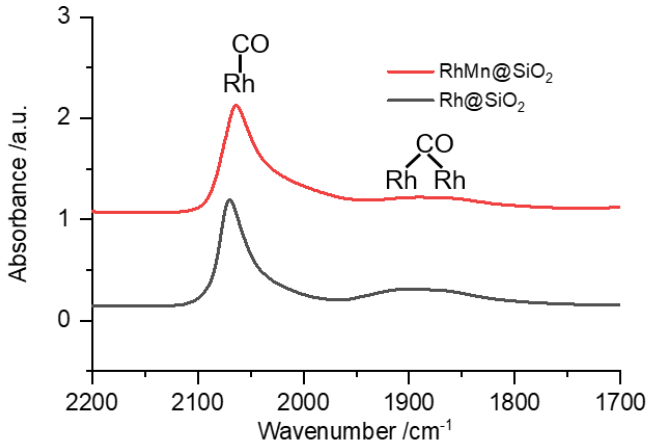

Figure S17. FTIR spectra of CO adsorbed on $Rh@SiO_2$ (black line) and $RhMn@SiO_2$ (red line) under 2.4 mbar CO pressure at room temperature.

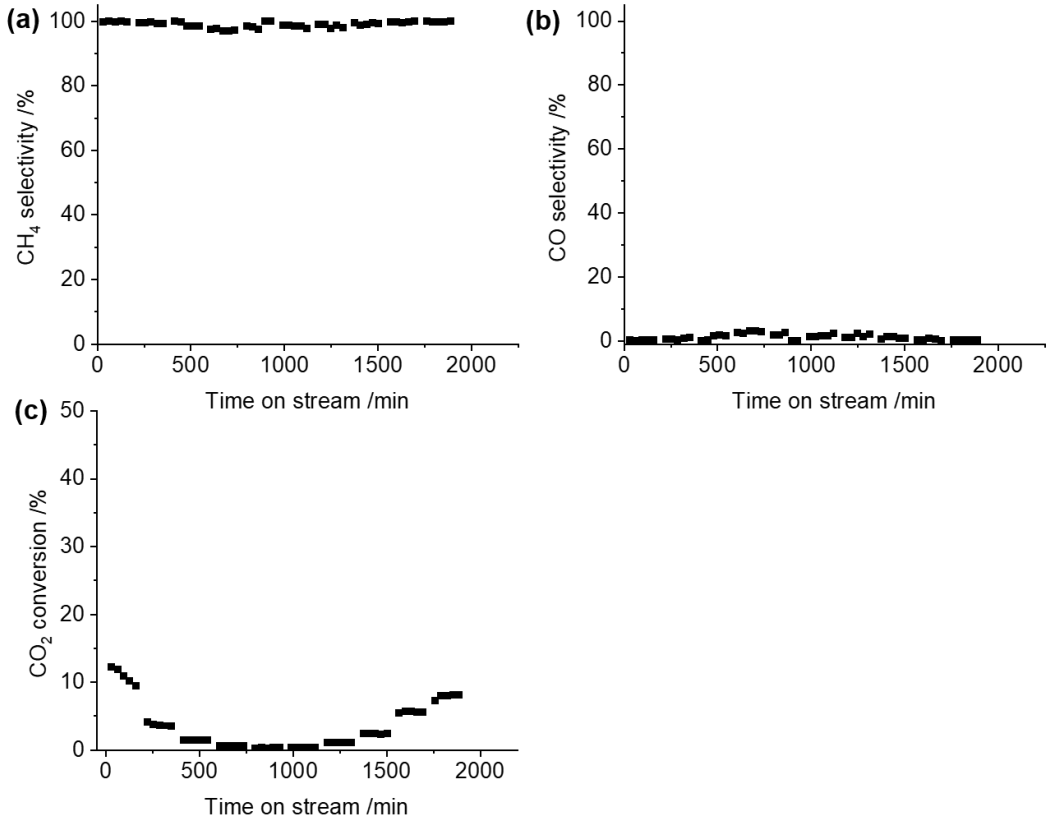

Figure S18. Catalytic performance of Rh@SiO_2 for CO_2 hydrogenation. (a) CH_4 selectivity, (b) CO selectivity and (c) CO_2 conversion. Reaction conditions: W_{cat} = 30 mg, F = 6-100 mL min^{-1}, T = 230 °C, P = 40 bar.

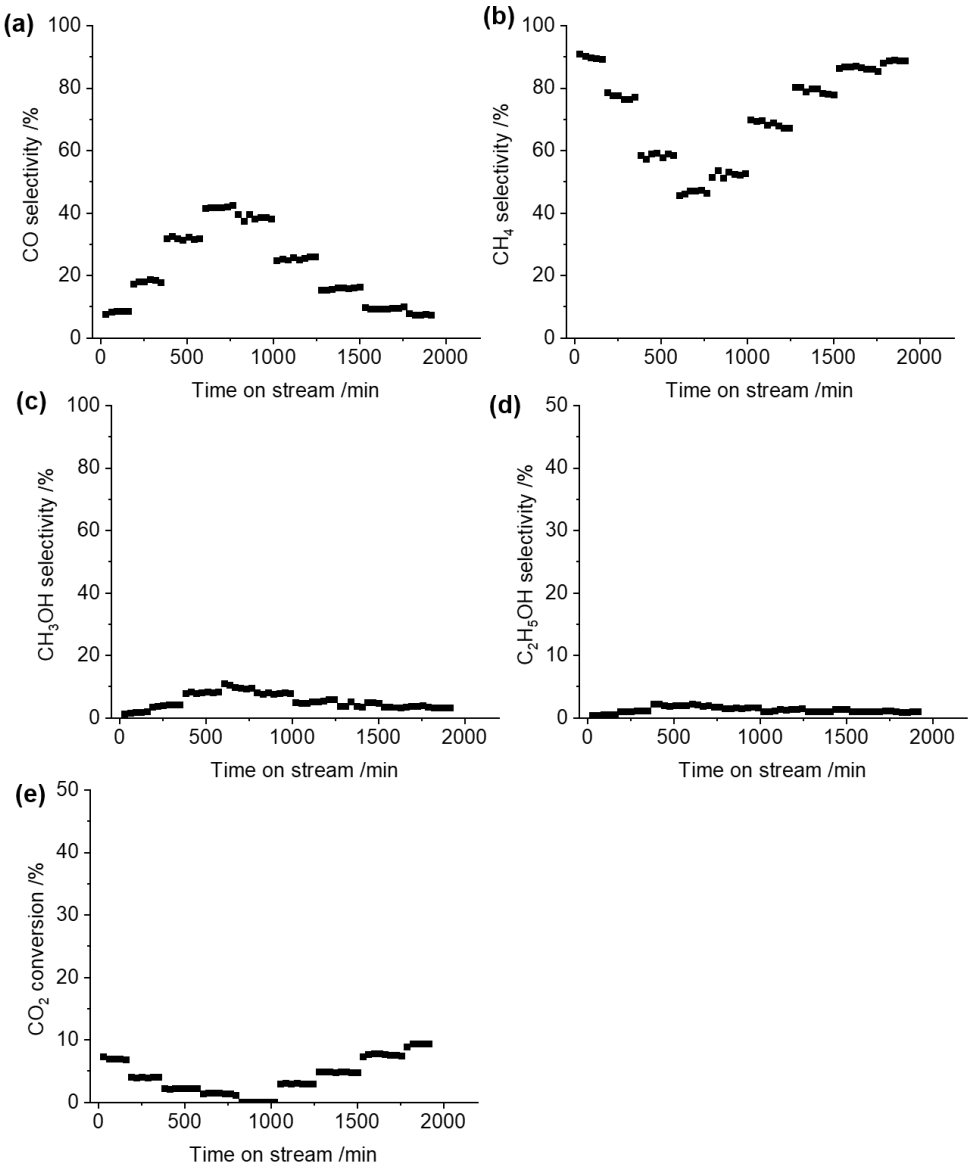

Figure S19. Catalytic performance of RhMn@SiO_2 for CO_2 hydrogenation. (a) CO selectivity, (b) CH_4 selectivity, (c) CH_3OH, (d) C_2H_5OH selectivity and (e) CO_2 conversion. Reaction conditions: W_{cat} = 125 mg, F = 6-100 mL min^{-1}, T = 230 °C, P = 40 bar.

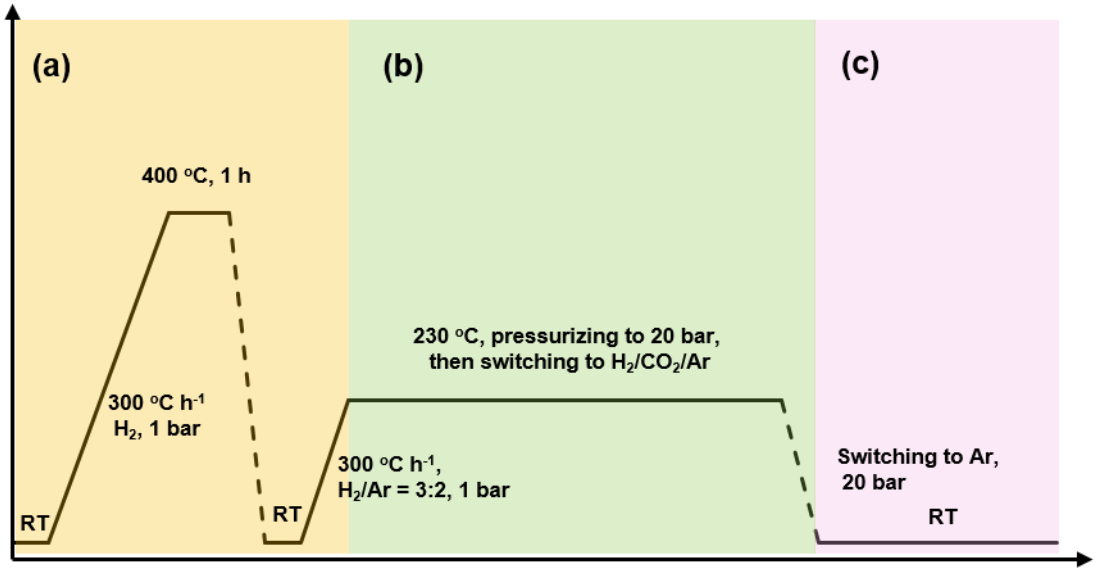

Figure S20. Scheme for the temperature/gas phase composition profile for a typical *in situ* XAS experiment.

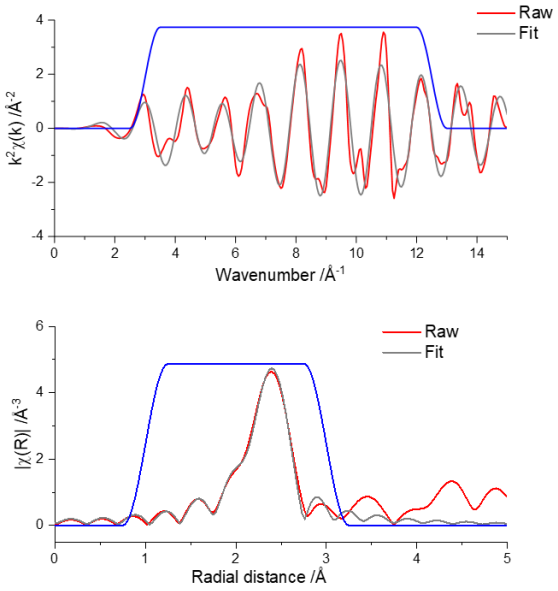

Figure S21. EXAFS fit for Rh foil (Rh K edge). Used to obtain amplitude reduction factor (S_0^2). (a) K-space with raw (red) and fitted (grey) data. Window (blue) 3.0-12.5 $Å^{-1}$, k-weight = 2, Hanning window, dk = 1; (b) R-space with raw (red) and fitted (grey) data. Window (blue) 1-3. Å, k-weight = 2, Hanning window, dk = 0.5. Fit summarized in table S1.

Table S2. Summary of Rh K-edge fitting results of Rh foil.[a]

Path	*N*	S_o^2	σ^2/Å^2	ΔE (eV)	R/Å	R-factor
Rh-Rh	12	0.85(0.06)	0.0034(0.0003)	-6.1(0.7)	2.68(0.01)	0.005

[a] 3.0 < k < 12.5, 1 < R < 3, k-weight = 2.

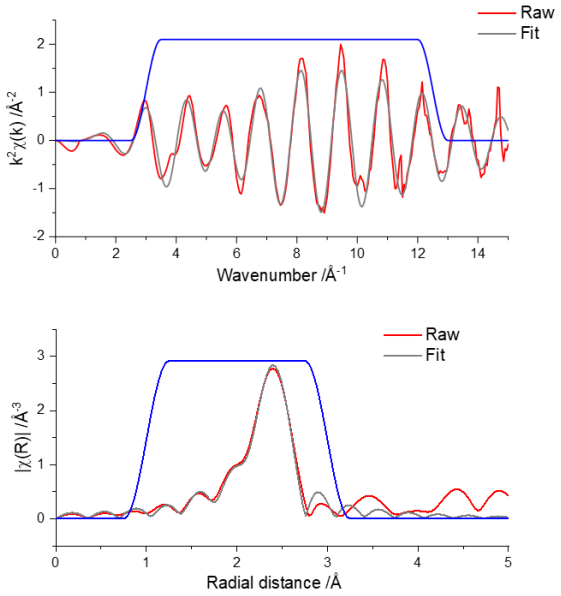

Figure S22. EXAFS fit for air exposed Rh@SiO_2. (a) K-space with raw (red) and fitted (grey) data. Window (blue) 3.0-12.5 Å^{-1}, k-weight = 2, Hanning window, dk = 1; (b) R-space with raw (red) and fitted (grey) data. Window (blue) 1-3. Å, k-weight = 2, Hanning window, dk = 0.5. Fit summarized in table S2.

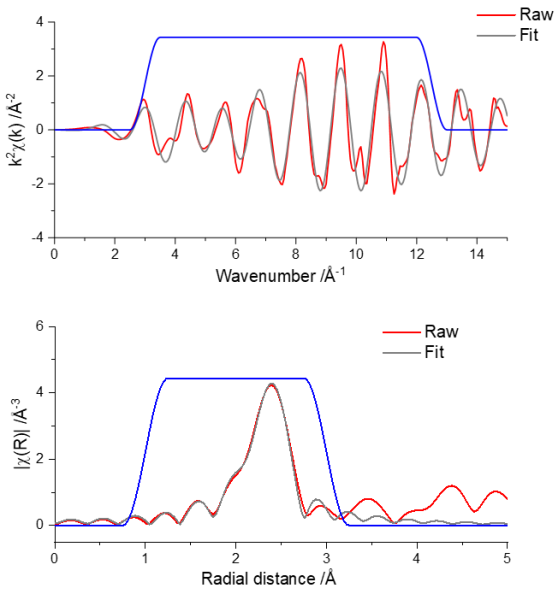

Figure S23. EXAFS fit for H_2 reduced Rh@SiO_2. (a) K-space with raw (red) and fitted (grey) data. Window (blue) 3.0-12.5 $Å^{-1}$, k-weight = 2, Hanning window, dk = 1; (b) R-space with raw (red) and fitted (grey) data. Window (blue) 1-3. Å, k-weight = 2, Hanning window, dk = 0.5. Fit summarized in table S2.

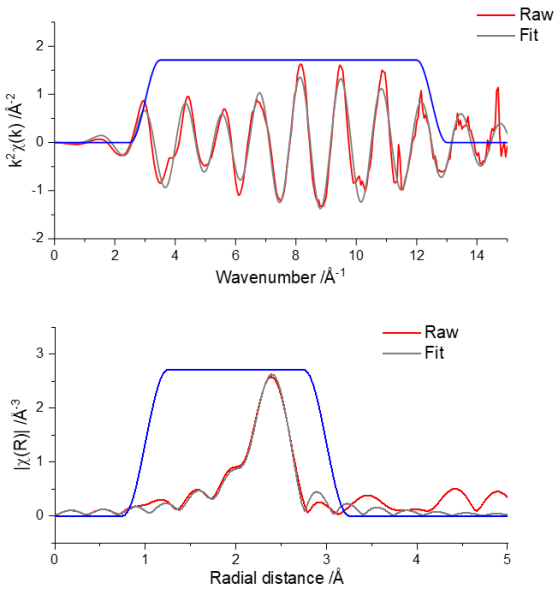

Figure S24. EXAFS fit for post CO_2 hydrogenation Rh@SiO_2. (a) K-space with raw (red) and fitted (grey) data. Window (blue) 3.0-12.5 $Å^{-1}$, k-weight = 1, Hanning window, dk = 1; (b) R-space with raw (red) and fitted (grey) data. Window (blue) 1-3. Å, k-weight = 2, Hanning window, dk = 0.5. Fit summarized in table S2.

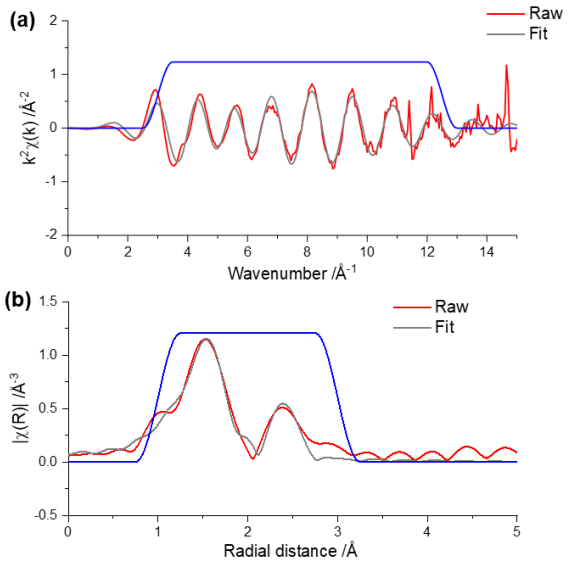

Figure S25. EXAFS fit for air exposed RhMn@SiO_2. (a) K-space with raw (red) and fitted (grey) data. Window (blue) 3.0-12.5 $Å^{-1}$, k-weight = 2, Hanning window, dk = 1; (b) R-space with raw (red) and fitted (grey) data. Window (blue) 1-3. Å, k-weight = 2, Hanning window, dk = 0.5. Fit summarized in table S2.

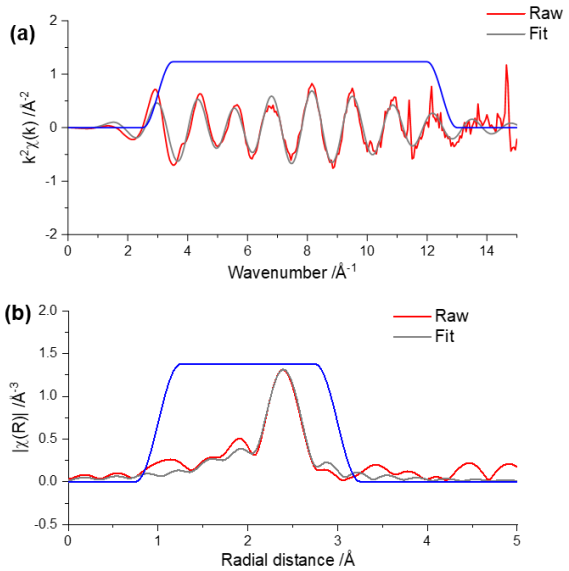

Figure S26. EXAFS fit for H_2 reduced RhMn@SiO_2. (a) K-space with raw (red) and fitted (grey) data. Window (blue) 3.0-12.5 $Å^{-1}$, k-weight = 2, Hanning window, dk = 1; (b) R-space with raw (red) and fitted (grey) data. Window (blue) 1-3. Å, k-weight = 2, Hanning window, dk = 0.5. Fit summarized in table S2.

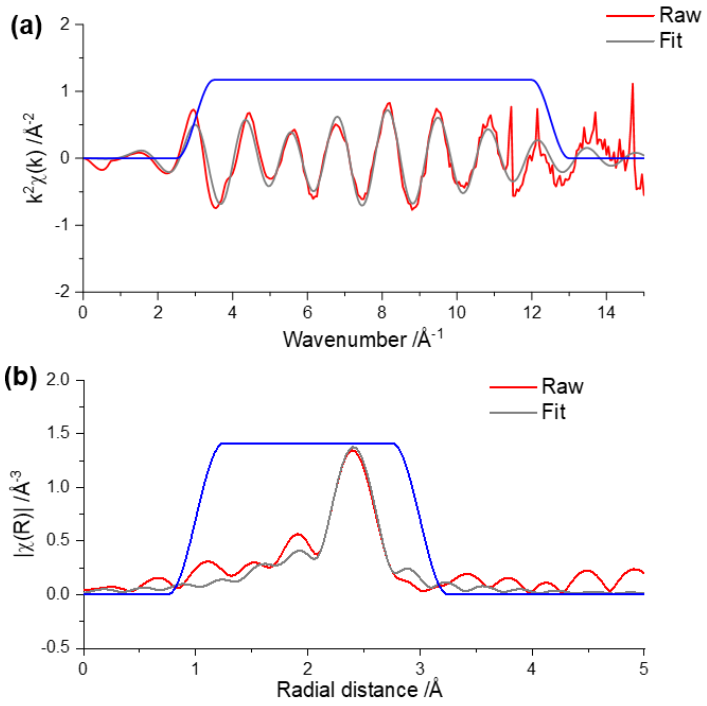

Figure S27. EXAFS fit for post CO_2 hydrogenation RhMn@SiO_2. (a) K-space with raw (red) and fitted (grey) data. Window (blue) 3.0-12.5 $Å^{-1}$, k-weight = 2, Hanning window, dk = 1; (b) R-space with raw (red) and fitted (grey) data. Window (blue) 1-3. Å, k-weight = 2, Hanning window, dk = 0.5. Fit summarized in table S2.

Table S3. Summary of Rh K-edge fitting results of Rh@SiO_2 and RhMnSiO_2 catalysts under different conditions.[a]

Catalyst	Conditions	Path	CN[b]	σ² (Å²)[c]	ΔE (eV)[d]	R (Å)[e]	R-factor
Rh@SiO_2	Air	Rh-Rh	8.7(0.7)	0.0046(0.0005)	-6.1 (0.7)	2.68(0.01)	0.009
	H_2 reduction	Rh-Rh	10.1(0.8)	0.0030(0.0004)	-5.9 (0.7)	2.68(0.01)	0.006
	Post CO_2 hydro.	Rh-Rh	8.6(0.7)	0.0051(0.0005)	-6.4 (0.7)	2.68(0.01)	0.009
RhMn@SiO_2	Air	Rh-Rh	2.2(1.4)	0.0078(0.0042)	-3.1 (2.7)	2.70(0.02)	0.037
		Rh-O	4.5(0.9)	0.0046(0.0022)	-3.1 (2.7)	2.03(0.02)	0.037
	H_2 reduction	Rh-Rh	6.4(0.8)	0.0079(0.0009)	-6.9 (1.0)	2.68(0.01)	0.016
	Post CO_2 hydro.	Rh-Rh	7.0(1.0)	0.0082(0.0010)	-6.4 (1.1)	2.68(0.01)	0.032

[a] 3.0 < k < 12.5; S_o^2 was fixed as 0.85 (from Rh foil); 1 < R < 3; k-weight = 2. [b] coordination number. [c] Debye-Waller parameter. [d] energy correction factor. [e] interatomic distance.

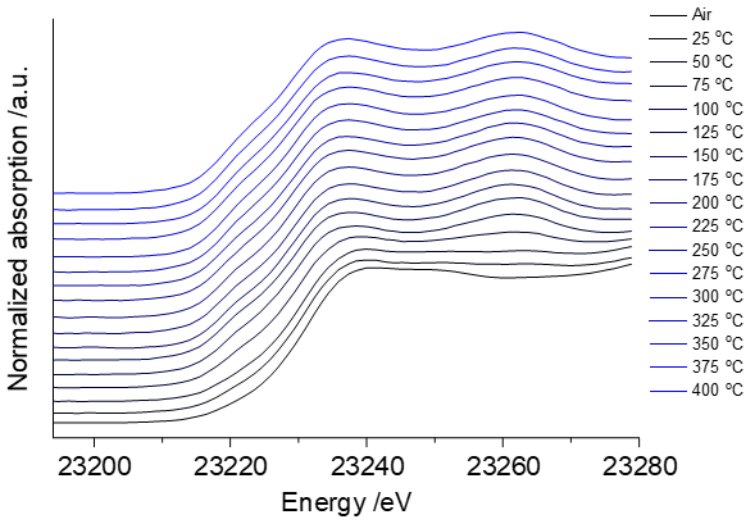

Figure S28. *In situ* XANES collected at Rh K-edge for RhMn@SiO_2 during H_2 temperature programmed reduction.

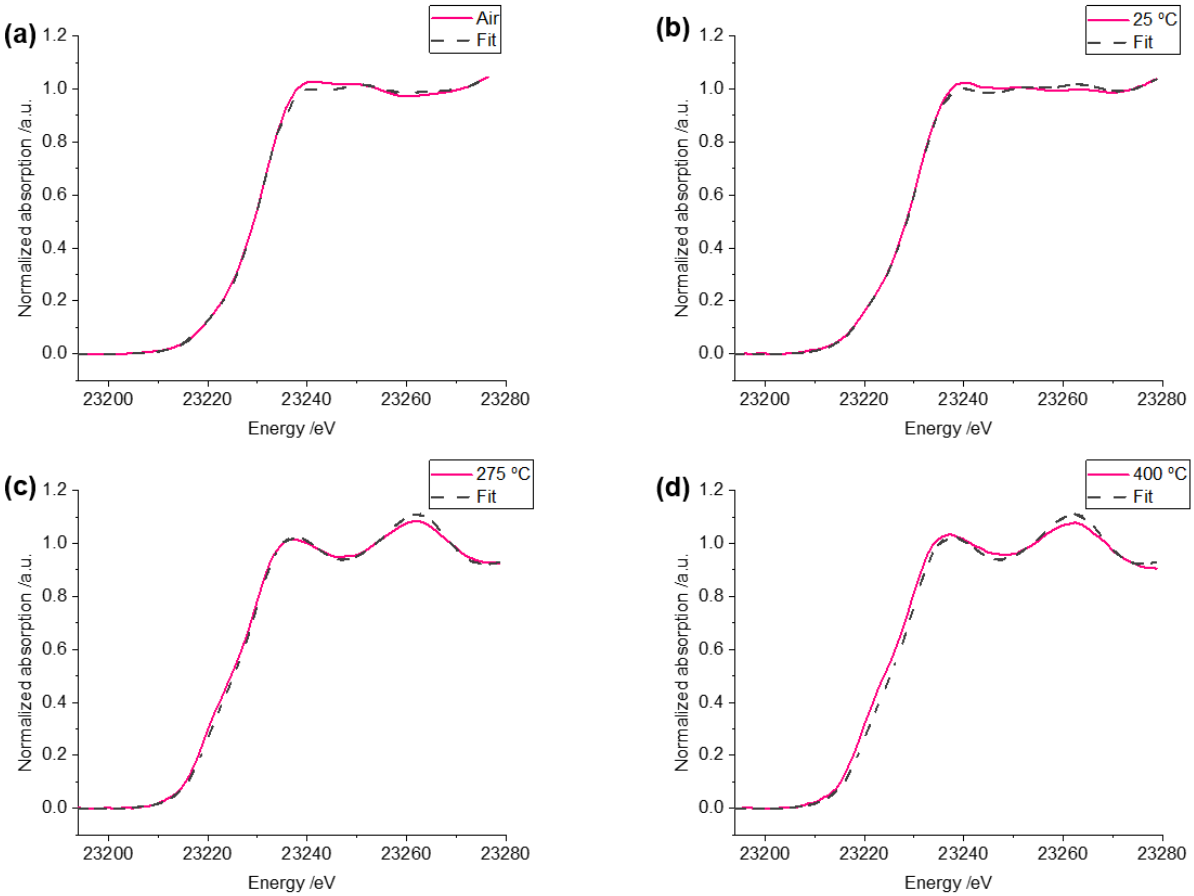

Figure S29. Representative linear combination fitting results of Rh K-edge XANES (a) air exposed, (b) H_2-TPR at 25 °C, (c) H_2-TPR at 275 °C and (d) H_2-TPR at 400 °C.

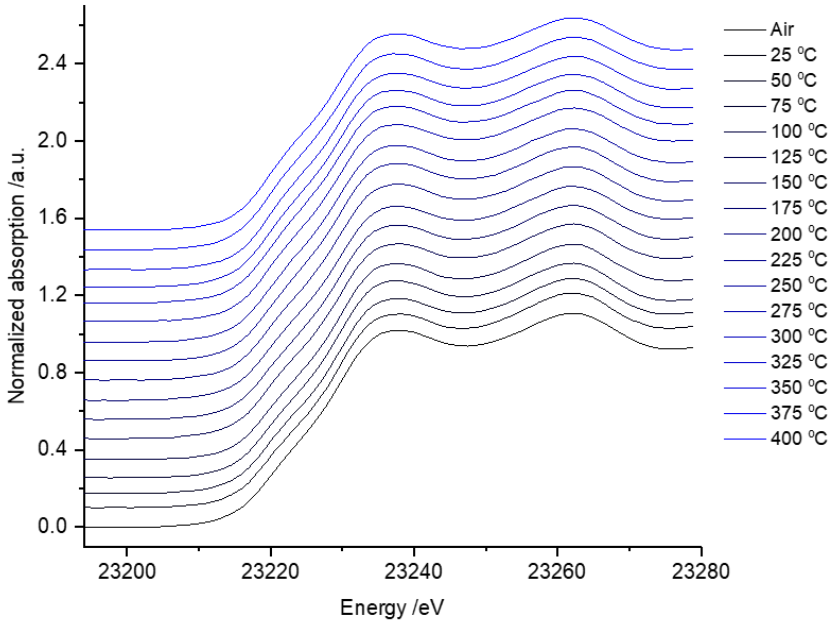

Figure S30. *In situ* XANES collected at Rh K-edge for Rh@SiO_2 during H_2 temperature programmed reduction.

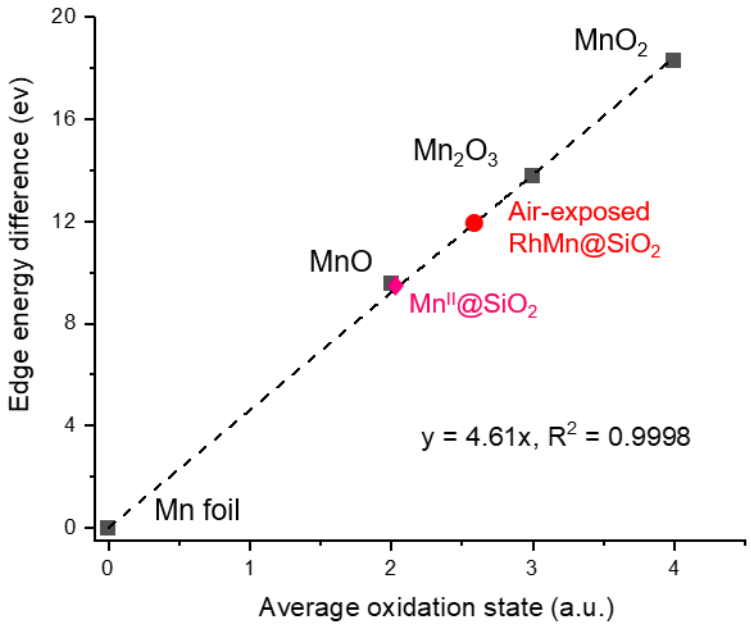

Figure S31. Average oxidation state as a function of difference on edge energy. The difference on edge energy are obtained by taking the value of the second peak of the first derivative EXAFS spectra of MnO, Mn_2O_3, and MnO_2 references minus 6539eV (the K-edge energy of Mn foil)

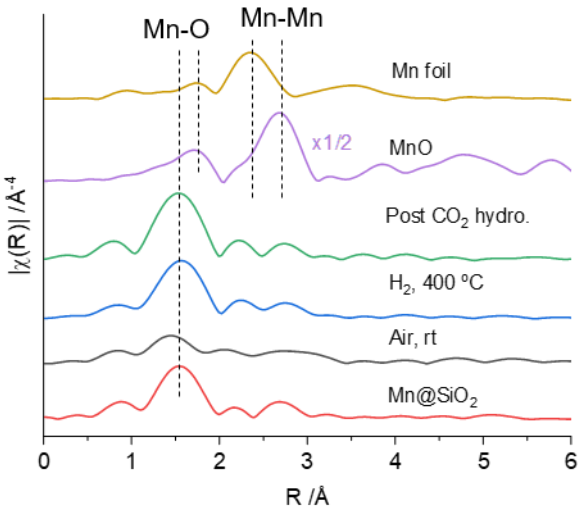

Figure S32. The k^3-weighted Fourier transforms of Mn K-edge EXAFS spectra for $RhMn@SiO_2$ under different conditions and reference samples.

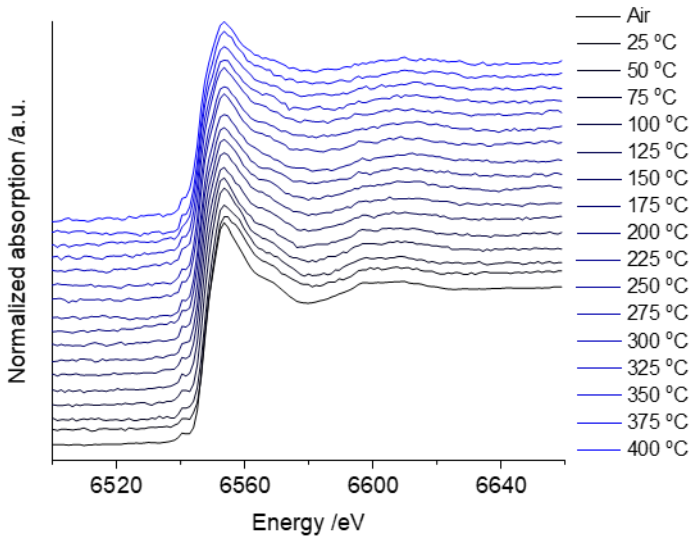

Figure S33. *In situ* XANES collected at Mn K-edge for Rh@SiO_2 during H_2 temperature programmed reduction.

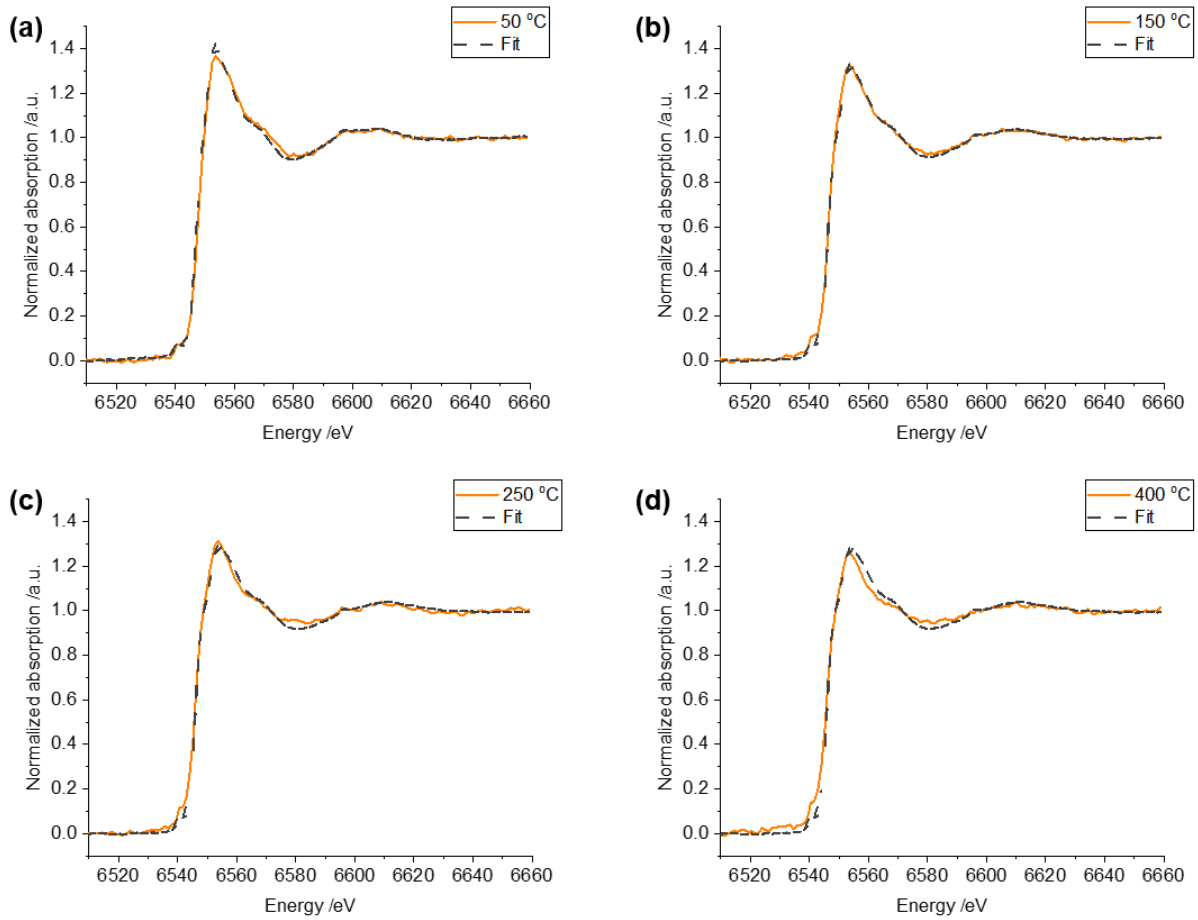

Figure S34. Representative linear combination fitting results of Mn K-edge XANES (a) H_2-TPR at 50 °C, (b) H_2-TPR at 150 °C, (c) H_2-TPR at 250 °C and (d) H_2-TPR at 400 °C.

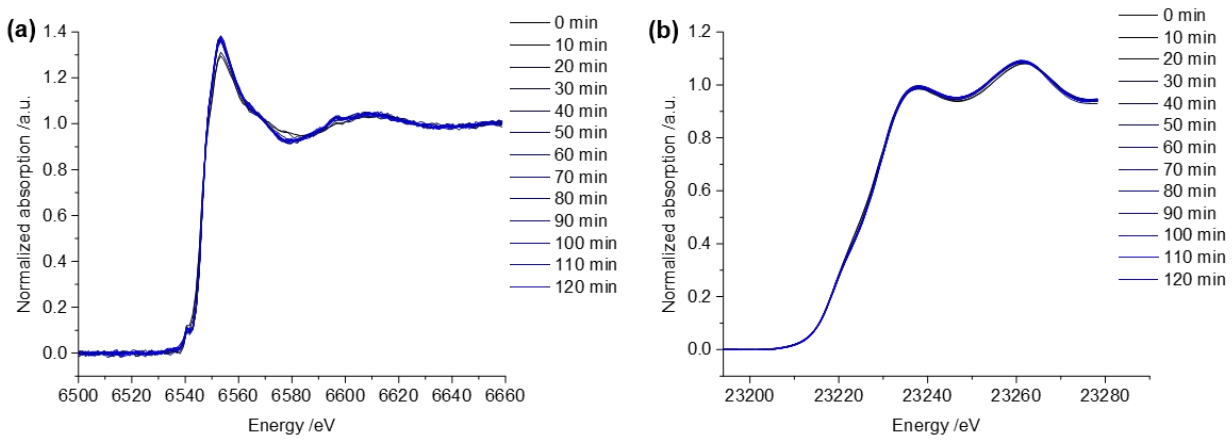

Figure S35. *In situ* XANES collected at Mn K-edge (a) and Rh K-edge (b) for RhMn@SiO_2 catalyst during CO_2 hydrogenation reaction.

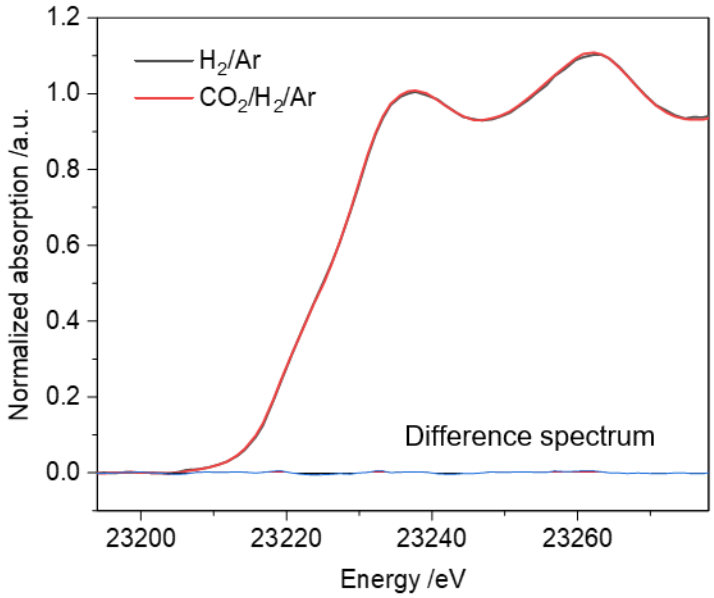

Figure S36. *In situ* Rh K-edge XANES spectra for Rh@SiO_2 catalyst collected under H_2/Ar (3:2, 20 bar) (black line) and under CO_2/H_2/Ar (1:3:1, 20 bar) after the reaction of 2 h (red line).

Reference:

[1] B. Ghaffari, J. Mendes-Burak, K. W. Chan, C. Copéret, *Chem. Eur. J.* **2019**, *25*, 13869-13873.

[2] H. Shoukang, S. Gambarotta, C. Bensimon, J. J. H. Edema, *Inorg. Chim. Acta* **1993**, *213*, 65-74.

[3] G. R. Fulmer, A. J. M. Miller, N. H. Sherden, H. E. Gottlieb, A. Nudelman, B. M. Stoltz, J. E. Bercaw, K. I. Goldberg, *Organometallics* **2010**, *29*, 2176-2179.

[4] P. J. Chupas, K. W. Chapman, C. Kurtz, J. C. Hanson, P. L. Lee, C. P. Grey, *J. Appl. Crystallogr.* **2008**, *41*, 822-824.

[5] K. A. Lomachenko, A. Y. Molokova, C. Atzori, O. Mathon, *J. Phy. Chem. C* **2022**, *126*, 5175-5179.

[6] B. Ravel, M. Newville, *J. Synchrotron Radiat.* **2005**, *12*, 537−541.

[7] O. V. Dolomanov, L. J. Bourhis, R. J. Gildea, J. A. K. Howard, H. Puschmann, *J. Appl. Cryst.* **2009**, *42*, 339-341.

[8] G. M. Sheldrick, *Acta Cryst.* **2015**, *A71*, 3-8.

[9] G. M. Sheldrick, *Acta Cryst.* **2015**, *C71*, 3-8.

[10] L. J. Bourhis, O. V. Dolomanov, R. J. Gildea, J. A. K. Howard, H. Puschmann, *Acta Cryst.* **2015**, *A71*, 59-75.